Mechanism for analogous illusory motion perception in flies and humans

Margarida Agrochao[a,1], Ryosuke Tanaka[b,1], Emilio Salazar-Gatzimas[b], and Damon A. Clark[a,b,c,d,2]

[a]Department of Molecular, Cellular and Developmental Biology, Yale University, New Haven, CT 06511; [b]Interdepartmental Neuroscience Program, Yale University, New Haven, CT 06511; [c]Department of Physics, Yale University, New Haven, CT 06511; and [d]Department of Neuroscience, Yale University, New Haven, CT 06511

Edited by John G. Hildebrand, University of Arizona, Tucson, AZ, and approved July 13, 2020 (received for review March 1, 2020)

Visual motion detection is one of the most important computations performed by visual circuits. Yet, we perceive vivid illusory motion in stationary, periodic luminance gradients that contain no true motion. This illusion is shared by diverse vertebrate species, but theories proposed to explain this illusion have remained difficult to test. Here, we demonstrate that in the fruit fly *Drosophila*, the illusory motion percept is generated by unbalanced contributions of direction-selective neurons' responses to stationary edges. First, we found that flies, like humans, perceive sustained motion in the stationary gradients. The percept was abolished when the elementary motion detector neurons T4 and T5 were silenced. In vivo calcium imaging revealed that T4 and T5 neurons encode the location and polarity of stationary edges. Furthermore, our proposed mechanistic model allowed us to predictably manipulate both the magnitude and direction of the fly's illusory percept by selectively silencing either T4 or T5 neurons. Interestingly, human brains possess the same mechanistic ingredients that drive our model in flies. When we adapted human observers to moving light edges or dark edges, we could manipulate the magnitude and direction of their percepts as well, suggesting that mechanisms similar to the fly's may also underlie this illusion in humans. By taking a comparative approach that exploits *Drosophila* neurogenetics, our results provide a causal, mechanistic account for a long-known visual illusion. These results argue that this illusion arises from architectures for motion detection that are shared across phyla.

vision | *Drosophila* | neural circuits | peripheral drift illusion

Visual illusions generate percepts that run counter to our reasoned expectations. They also provide windows into the function of our visual systems (1). Among the most surprising are motion illusions that can generate the perception of motion in patterns that are in fact stationary. In humans, robust motion percepts are elicited by periodic sawtooth luminance gradients (2, 3) (Fig. 1*A* and Movie S1) or by periodic chromatic patterns (4), and these percepts are called peripheral drift illusions. The same stationary patterns have been reported to elicit illusory motion percepts across diverse vertebrate species, including nonhuman primates (5), cats (6), and fish (7).

Two hypotheses have been proposed to explain the illusion in vertebrates, based on mechanisms either upstream or downstream of motion detection. The first hypothesis argues that stimuli with higher contrast or luminance are processed faster, so that different locations in a luminance gradient appear to be presented sequentially, generating an illusion of motion (2, 9). The second hypothesis attributes the illusion to retinal motion resulting from microsaccades (10, 11). Physiological and psychophysical evidence provides correlational evidence for both hypotheses (9–11), but they have remained difficult to test directly.

We set out to study this motion illusion in the fruit fly *Drosophila*, where powerful genetic tools make it possible to causally connect visual perception to activity in specific neurons. The motion detection circuitry in flies has been studied extensively by leveraging genetic and anatomical tools (12), and their motion detection algorithm has many parallels with vertebrate motion detection (13). Photoreceptors in the fly's retina detect light and downstream circuits split into ON and OFF pathways, which also process signals in space and time. Motion is first detected in the direction-selective neurons T4 and T5, which respond exclusively to moving light or dark edges, respectively (14). The neurons T4 and T5 are required for motion-dependent behaviors, including optomotor turning (14), walking-speed regulation (15), and loom detection (16).

In this study, by combining behavioral measurements, genetic silencing, and neural imaging, we find that flies, like vertebrates, perceive illusory motion in stationary images, and that the illusion requires motion detection circuitry. Using neural imaging, we find that T4 and T5 neurons with opposite direction preferences encode the sharp edges of the sawtooth pattern in a complementary manner. We show that this edge encoding can arise in a variety of computational models for motion detection. We propose a mechanism for this illusion based on an imbalance between light and dark motion detection, and find support for it in flies by selectively silencing light or dark edge motion detectors. Since the same mechanism could plausibly exist in humans, we also devised psychophysical tests of the model in humans. The results of these tests are consistent with similar mechanisms underlying this motion illusion in humans. Our findings highlight several components of motion detection underlying the illusion—the splitting of ON and OFF motion pathways, their imbalanced contributions to behavior, and motion opponency—that likely

Significance

Most of the time, visual circuitry in our brains faithfully reports visual scenes. Sometimes, however, it can report motion in images that are in fact stationary, leading us to perceive illusory motion. In this study, we establish that fruit flies, too, perceive motion in the stationary images that evoke illusory motion in humans. Our results demonstrate how this motion illusion in flies is an artifact of the brain's strategies for efficiently processing motion in natural scenes. Perceptual tests in humans suggest that our brains may employ similar mechanisms for this illusion. This study shows how illusions can provide insight into visual processing mechanisms and principles across phyla.

Author contributions: M.A., R.T., E.S.-G., and D.A.C. designed research; M.A., R.T., and E.S.-G. performed research; M.A., R.T., E.S.-G., and D.A.C. analyzed data; and M.A., R.T., and D.A.C. wrote the paper.

The authors declare no competing interest.

This article is a PNAS Direct Submission.

Published under the PNAS license.

[1]M.A. and R.T. contributed equally to this work.

[2]To whom correspondence may be addressed. Email: damon.clark@yale.edu.

This article contains supporting information online at https://www.pnas.org/lookup/suppl/doi:10.1073/pnas.2002937117/-/DCSupplemental.

First published August 24, 2020.

Downloaded at Palestinian Territory, occupied on December 6, 2021

www.manaraa.com

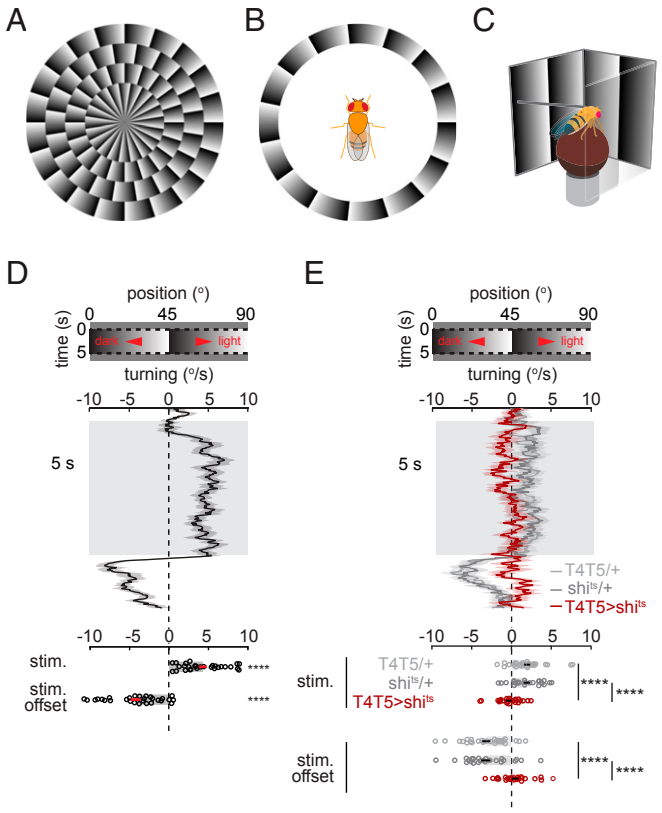

Fig. 1. *Drosophila* perceive illusory motion in stationary sawtooth gradients. (*A*) Circularly arranged sawtooth gradients elicit clockwise motion percepts in human observers (2, 3). See also Movie S1. (*B*) In fly experiments, the gradients were arranged about the fly to induce the impression of yaw rotation. (*C*) To measure fly turning behavior, tethered flies were placed above air-supported balls while sawtooth gradients were projected onto panoramic screens (8). (*D* and *E*, *Top*) Space–time plot of the sawtooth gradients. (*D* and *E*, *Middle*) Time traces of average turning responses of (*D*) wild-type flies (see *SI Appendix* for genotype) (n = 29 flies) or (*E*) T4- and T5-silenced flies (T4T5>shi^{ts}, red; n = 24) and respective control flies for T4T5-Gal4 (T4T5/+, lighter gray; n = 28) and UAS-shibire^{ts} (shi^{ts}/+, darker gray; n = 24) (mean ± SEM). (*D* and *E*, *Bottom*) Time-averaged responses during or at the offset of the sawtooth gradient presentation. Error bars indicate mean ± SEM. ****$P \leq 0.0001$ by (*D*) Wilcoxon signed-rank tests against 0 or (*E*) Wilcoxon rank-sum tests across flies.

reflect constraints imposed by biology and by the common visual environment shared by sighted animals.

Results

***Drosophila* Perceive Illusory Motion in Stationary Sawtooth Gradients.** When walking flies are presented with a full-field visual stimulus rotating in the horizontal plane, they turn in the direction of the stimulus rotation, a behavior called optomotor turning (17, 18). We hypothesized that, if flies perceive motion in stationary sawtooth gradients, that stimulus might also trigger optomotor turning if it were arrayed azimuthally around the fly (Fig. 1*B*). To monitor fly turning responses to stationary sawtooth gradients, a tethered fly was placed above an air-supported ball while the visual stimulus was presented on surrounding panoramic screens (Fig. 1*C*). The turning response was then measured by the rotation of the ball.

When stationary sawtooth gradients with a 45° period were presented for 5 s, flies exhibited slow, sustained average turning toward the lighter shade along the shallow gradient (Fig. 1*D*). The observed turning was canceled when the sawtooth gradient rotated at ∼1.5 °/s in the opposite direction (*SI Appendix*, Fig. S1). At stimulus offset, flies turned transiently in the opposite direction (Fig. 1*D*). The directionality of turning, the sustained bias in turning, and the offset response all agree with the phenomenology of the illusory motion perception evoked in humans by stationary sawtooth gradients (2, 19). Insects perceive illusory motion in temporally oscillating sawtooth gradients (20), but it remained unclear whether they perceive motion in purely stationary stimuli as well.

The optomotor turning response depends on neurons that detect motion (14), but flies also turn in response to other visual cues, for instance while tracking objects (21) or navigating toward light (22). To test whether the observed turning reflected the output of motion detection circuitry, we expressed *shibire^{ts}*, a dominant suppressor of synaptic transmission (23), in T4 and T5, the most peripheral direction-selective neurons in the fly brain. This silencing abolishes the optomotor turning response (14) but not object tracking (21). With T4 and T5 neurons silenced, flies turned significantly less in response to the stationary sawtooth gradients (Fig. 1*E*), demonstrating that the observed turning relies on motion detection.

T4 and T5 Neurons Respond to Spatial Contrast Edges in a Direction- and Polarity-Specific Manner. Since T4 and T5 neurons are required for flies to perceive motion in stationary sawtooth gradients, we next asked how these neuron types responded to this stimulus. We used two-photon microscopy to measure neural activity in T4 and T5 neurons expressing the calcium indicator GCaMP6f (24) while presenting the panoramic visual stimulus (8, 25) (Fig. 2*A*). The neurons T4 and T5 respond preferentially to motion of light and dark edges, respectively (14) (Fig. 2*B*). At each point in visual space, there are four subtypes of T4 and T5 neurons, with each type sensitive to motion in one of the four cardinal directions. The four neuron types that encode motion in the horizontal plane are T4a and T5a (front-to-back motion) and T4b and T5b (back-to-front motion) (Fig. 2*C*). We identified their spatial receptive field (RF) centers by presenting 5°-wide white or black vertical bars at various azimuthal locations (26, 27) (*SI Appendix*). T4 neurons responded exclusively to white bars and T5 neurons to black bars, as expected from previous measurements (26–29) (Fig. 2*D*).

Next, we presented horizontal, stationary sawtooth gradients with various displacements relative to the RF centers (Fig. 2*E*). The neurons responded to the stationary periodic patterns (28), but with a distinctive spatial pattern. First, the responses were localized about sharp contrast edges rather than the regions of shallow gradients. Second, each neuron responded only when its preferred contrast (light for T4 neurons, dark for T5 neurons) was located at its RF center. Third, both neuron types responded most strongly when their nonpreferred contrast (dark for T4 neurons, light for T5 neurons) was presented toward their preferred direction relative to their RF center. For example, the neuron T4a, which prefers light edges moving front to back, responded most when a dark contrast flanked its RF center on the back (preferred direction) side (Fig. 2 *E*, *Left*). In this way, each neuron type responded most to the stationary version of its preferred moving edge (Fig. 2*G* and Movie S2). For example, the neuron T4a responded more to stationary edges that had light contrast on the front side and dark contrast on the back side—a snapshot of the moving edge it prefers—compared with ones with the opposite polarity. As a consequence, each stationary contrast edge is encoded most strongly by a pair of motion detectors with opposite polarity preference (light vs. dark) and opposite direction preference (front to back vs. back to front) (Fig. 2*E*). The pattern of T4 and T5 neurons' responses to stationary edges generalized to other visual stimuli, including stationary square-wave gratings (Fig. 2*F* and *SI Appendix*, Fig. S2*A*) and naturalistic contrast patterns (*SI Appendix*, Fig. S2*B*). In these responses, the four cell types each

Downloaded at Palestinian Territory, occupied on December 6, 2021
www.manaraa.com

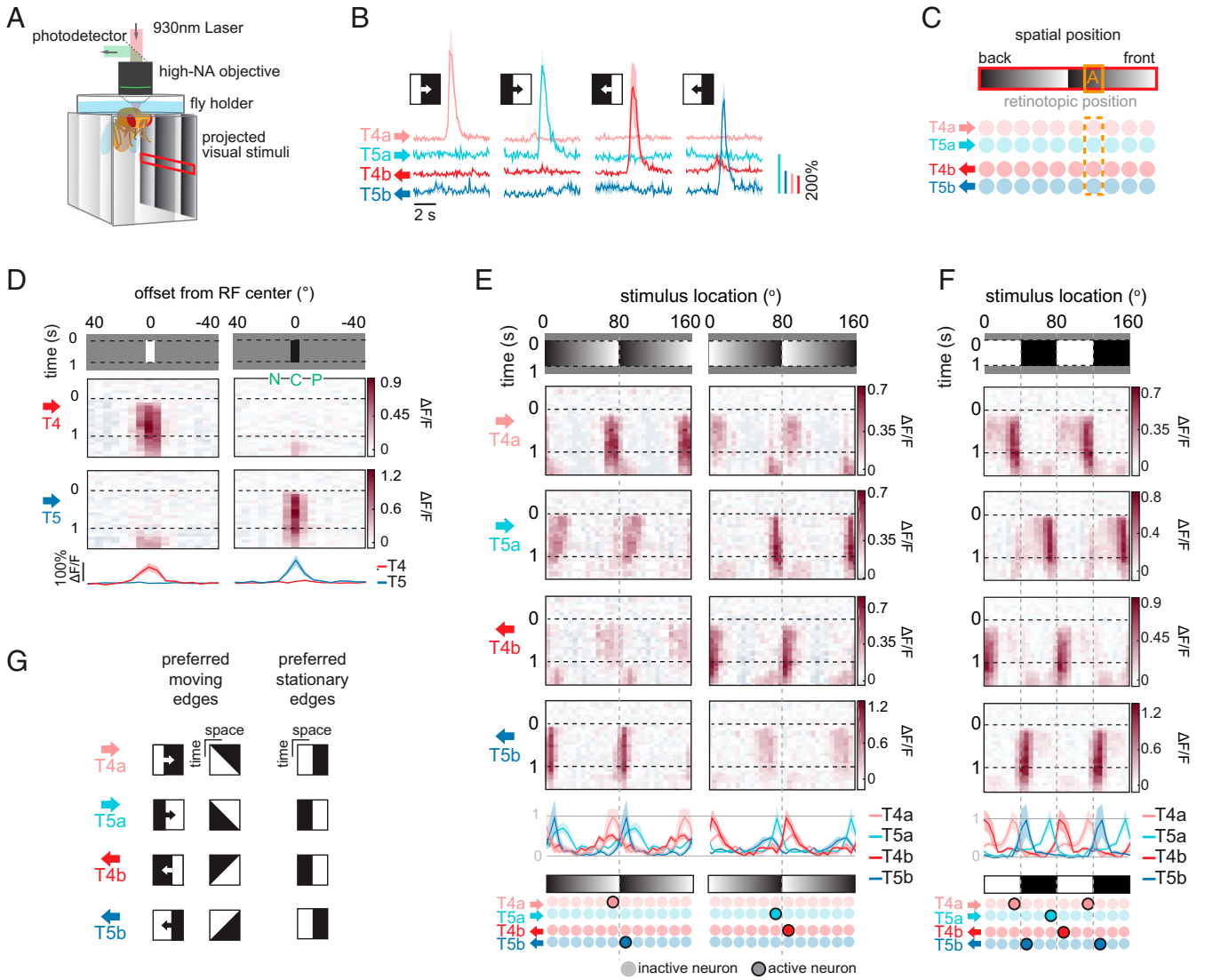

Fig. 2. T4 and T5 neurons respond to spatial contrast edges in a direction- and polarity-specific manner. (*A*) Imaging setup for measuring neural responses from T4 and T5 neurons. NA, numerical aperture. (*B*) Calcium responses of T4 and T5 neurons to moving edges. Edges were either light (first and third columns) or dark (second and fourth columns), and moved front to back (first two columns) or back to front (second two columns) around the fly. (*C*) At each retinotopic position (point A in orange box), motion in the horizontal plane is encoded by T4a, T5a, T4b, and T5b neurons. Rows of circles indicate arrays of T4 and T5 neurons tiling horizontal visual space. (*D*) Calcium responses of T4 and T5 neurons to a 5°-wide light or dark bar (*Top*) over space and time and (*Bottom*) over space, time-averaged (mean ± SEM). Henceforth, each column of space–time response plots represents the calcium response of cells whose RF center was at the stimulus location indicated by the *x* axis (*SI Appendix*). Subtypes of T4 and T5 neurons were averaged such that their preferred direction points rightward in the figure; n = 10, 10, 7, and 6 flies for T4a, T4b, T5a, and T5b neurons, respectively. Also indicated are the center (C), preferred (P), and null (N) sides of the RF. (*E*, *Top*) Calcium responses of T4a, T5a, T4b, and T5b neurons to 1-s presentation of stationary sawtooth luminance stimuli. Gradient luminance increases in the front-to-back direction (*Left*) or in the back-to-front direction (*Right*). (*E*, *Middle*) Time-averaged responses of each neuron (mean ± SEM). The time-averaged responses are normalized within each cell type. (*E*, *Bottom*) Cartoon showing which neurons are most activated by the two sawtooth stimuli. Highlighted circles indicate neurons that are activated by the stimulus; n = 7, 4, 2, and 6 flies for T4a, T4b, T5a, and T5b neurons, respectively. (*F*, *Top*) Calcium responses of T4a, T5a, T4b, and T5b neurons to 1-s presentation of stationary square-wave gratings. (*F*, *Middle*) Time-averaged responses as in *E*. (*F*, *Bottom*) Summary of responses as in *E*. The time-averaged responses are normalized within each cell type; n = 10, 10, 7, and 6 flies for T4a, T4b, T5a, and T5b neurons, respectively. (*G*) A space–time schematic comparing the preferred moving and stationary edge stimuli for each cell type. The preferred stationary edges of T4 and T5 are the stationary versions of their preferred moving edges (Movie S2).

respond to nonoverlapping stimulus features, consistent with a decorrelated stimulus encoding (27).

Responses to Stationary Edges Emerge through Different Phenomenology in T4 and T5 Neurons. Next, we investigated how the observed stationary edge responses in T4 and T5 neurons might arise. The calcium responses of T4 and T5 neurons are shaped by contrast at their RF centers, but also by the contrasts flanking the center (25, 27, 30, 31). To begin to dissociate the contributions of contrasts at different regions of the RF, we presented stationary square-wave gratings that only included either contrast decrements (gray–black) or increments (gray–white) (Fig. 3*A* and *SI Appendix*, Fig. S3*A*).

T4 neurons showed edge-specific responses to the gray–black square-wave grating (Fig. 3*A*) similar to responses to the white–black grating (Fig. 2*F*), although with a smaller magnitude. However, surprisingly, their responses to the gray–white grating were weaker and not edge-specific (Fig. 3*A* and *SI Appendix*, Fig. S3*A*).

Downloaded at Palestinian Territory, occupied on December 6, 2021
www.manaraa.com

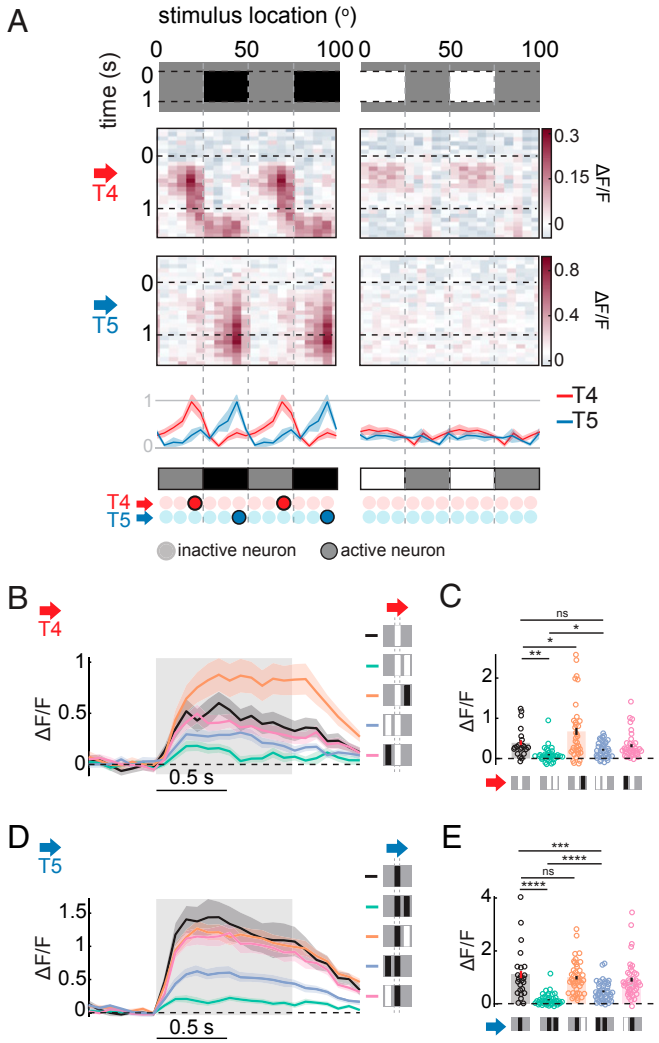

Fig. 3. Responses to stationary edges emerge through different phenomenology in T4 and T5 neurons. (*A*) Calcium responses of T4 and T5 neurons to 1-s presentation of half-contrast square-wave gratings, gray to black (*Left*) or white to gray (*Right*). (*A*, *Bottom*) Time-averaged responses of T4 and T5 neurons over space, normalized within each cell type (mean ± SEM), and a summary of the responses, similar to Fig. 2 *E* and *F*. The responses of subtypes of T4 and T5 neurons were averaged so that their preferred direction points rightward in the figures; $n = 10$, 8, 2, and 4 flies for T4a, T4b, T5a, and T5b neurons, respectively. (*B*–*E*) Calcium response of (*B* and *C*) T4 and (*D* and *E*) T5 neurons to 1-s presentation of stationary single or paired bars. A preferred contrast bar was presented at the neurons' RF center in all conditions, which was accompanied by another black or white bar, separated 10° (center to center) to either side of the RF. Responses of subtypes of T4 and T5 neurons were averaged so that their preferred directions point rightward in the figure. (*B* and *D*) Time traces of the calcium responses. (*C* and *E*) Time-averaged responses. All are mean ± SEM; $n = 21$, 14, 24, and 18 flies for T4a, T4b, T5a, and T5b neurons, respectively. Bars with error bars indicate mean ± SEM. $^*P \le 0.05$, $^{**}P \le 0.01$, $^{***}P \le 0.001$, $^{****}P \le 0.0001$ by a Wilcoxon rank-sum test across flies. ns, nonsignificant.

T5 neurons also showed edge-specific responses to the gray–black grating (Fig. 3*A* and *SI Appendix*, Fig. S3*A*), similar to responses to the white–black grating (Fig. 2*F*). They did not respond strongly to the gray–white grating (Fig. 3*A* and *SI Appendix*, Fig. S3*A*), as expected from their preference for dark contrast. These results suggest that asymmetric mechanisms underlie stationary edge responses in T4 and T5. While nonpreferred contrast on the preferred side of the RF is necessary for T4 neurons to show stationary edge responses, preferred contrast on the null side alone is sufficient for T5 neurons' stationary edge responses.

To further investigate how contrasts flanking the RF center affect responses of T4 and T5 neurons, we presented simultaneous pairs of 5°-wide bars. The bars were either light or dark, and positioned 10° apart from each other. We repeated the presentation of the bar pairs at various azimuthal locations, and examined how the presence of the second bar modulated the responses of T4 and T5 neurons to a single bar with preferred contrast at the RF center (Fig. 3 *B*–*E* and *SI Appendix*, Fig. S3 *B*–*I*).

For T4 neurons, when the second bar was light, it significantly suppressed the response only when it was on the preferred side (Fig. 3 *B* and *C* and *SI Appendix*, Fig. S3 *B*–*E*), consistent with previous measurements (26, 27, 30). Moreover, when the second bar was dark, it enhanced responses only when it was on the preferred side (Fig. 3 *B* and *C* and *SI Appendix*, Fig. S3 *B*–*E*), consistent with its response to the gray-to-dark grating. For T5 neurons, when the second bar was dark on either side of the RF center, it significantly suppressed the response, with stronger suppression by the preferred side bar (Fig. 3 *D* and *E* and *SI Appendix*, Fig. S3 *F*–*I*), similar to T4. This spatially asymmetric inhibition in T5 is consistent with previous measurements (27, 29, 32), and is sufficient to explain its responses to square-wave gratings (Fig. 3*A* and *SI Appendix*, Fig. S3*A*). In contrast to T4, T5 responses were not enhanced when the second bar was the nonpreferred contrast (Fig. 3 *D* and *E* and *SI Appendix*, Fig. S3 *F*–*I*).

A Minimal Synaptic Model of T4 Captures the Stationary Edge Responses. Next, we wondered whether a simple synaptic model of T4 (33) (Fig. 4 *A*, *Top*) could capture the basic phenomenology of T4 neurons' stationary edge responses. The model is equipped with three spatially displaced input arms, each corresponding to anatomically and physiologically characterized input neuron types to T4 (27, 34–37). The membrane voltage of the model T4 neuron is computed based on synaptic conductances modulated by the three input arms (*SI Appendix*) (26, 38). Although we did not have a comparable, thoroughly characterized synaptic model for T5, we nonetheless implemented one under the same design principle as the T4 model (*SI Appendix*, Fig. S4).

With an appropriate choice of the temporal filters on its input arms, the minimal synaptic model of T4 qualitatively replicated the spatial pattern of T4's response to stationary sawtooth patterns and square-wave gratings—namely, the model responded strongly only when light contrast was on its RF center and dark contrast was on the preferred side (Fig. 4 *B*, *Top*). It also reproduced T4's responses to the pairs of bars (Fig. 4 *D*, *Top*). On the other hand, the model did not respond to the gray–black square-wave grating (Fig. 4 *C*, *Top*) and its response to the white–gray grating was similar to its response to the white–black grating (Fig. 4 *C*, *Top*), unlike the corresponding physiological results (Fig. 3*A* and *SI Appendix*, Fig. S3*A*).

The insensitivity of the model to the gray–black grating is expected from its design, since the model lacks excitatory OFF inputs (Fig. 4 *A*, *Top*). To implement T4's sensitivity to contrast decrements, we introduced baseline activity to the arm on the preferred side, which represents inhibitory ON neurons, most likely Mi4 or CT1 (27, 33–36, 41) (Fig. 4 *A*, *Bottom*). Such baseline activity in this arm allows it to reduce activity in the presence of dark contrasts, thereby disinhibiting T4. When we introduced a small positive bias to the preferred side arm of the model, it indeed showed edge-selective responses to the gray–black square-wave grating (Fig. 4 *C*, *Bottom*), as well as reduced responses to the gray–white square-wave gratings (Fig. 4 *C*, *Bottom*), similar to physiological results (Fig. 3 *A* and *SI Appendix*, Fig. S3*A*). This modification did not compromise basic response properties of the model (Fig. 4 *B* and *D* and *SI Appendix*, Fig. S4 *E* and *F*).

Downloaded at Palestinian Territory, occupied on December 6, 2021
www.manaraa.com

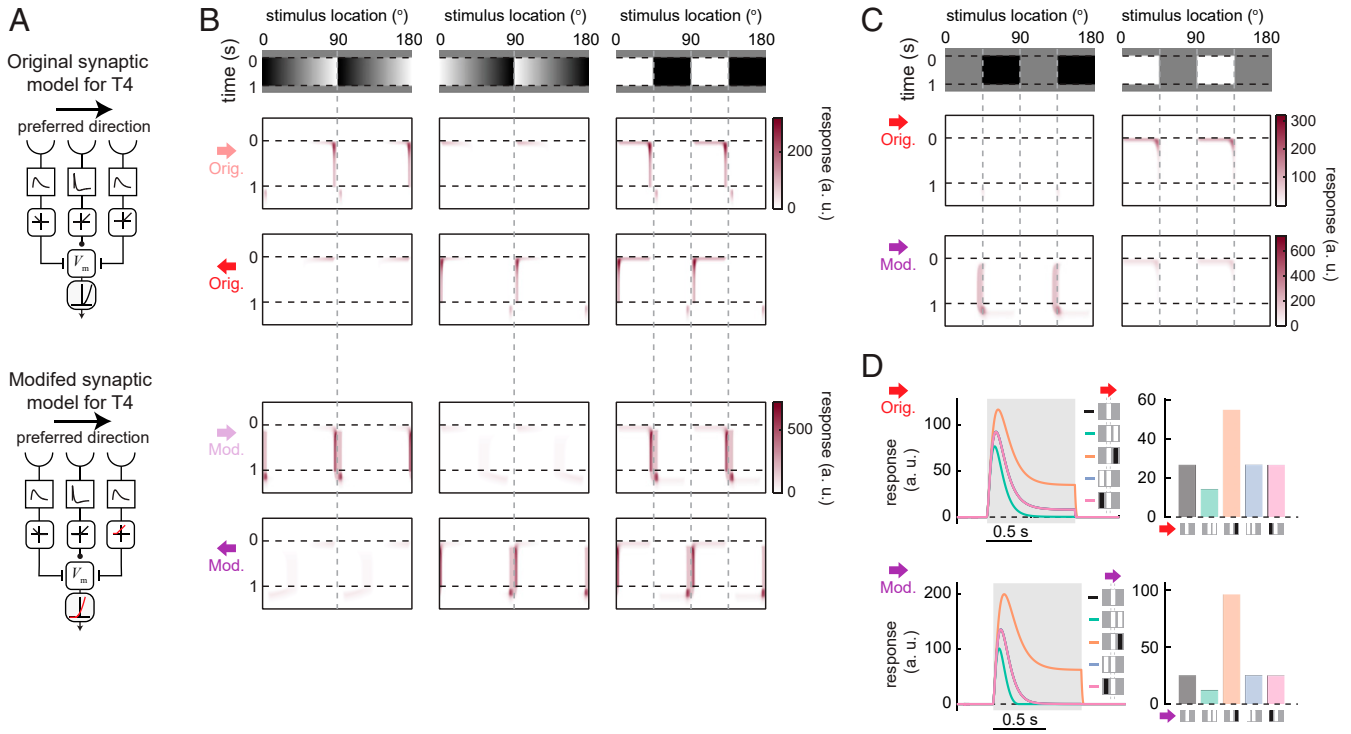

Fig. 4. Minimal synaptic model replicates the stationary edge responses of T4. (*A*) Minimal synaptic models of T4 neurons (33, 39), based on the anatomy and physiology of the T4 circuit, (*Top*) without or (*Bottom*) with a modification to introduce a positive bias term into the output of the preferred side branch. In the modified model, a bias term was also added to the membrane voltage to offset the effect of constitutive inhibition from the preferred side arm. The models have three spatially separated input branches. The side branches undergo temporal low-pass filtering, whereas the middle undergoes high-pass filtering. After the sign of the left branch is reversed, the outputs of all the branches are half-wave–rectified. The outputs of the three branches are then treated as either inhibitory (left and right branches) or excitatory (middle branch) synaptic conductances onto T4 neurons (*SI Appendix*). Transformation from membrane voltage to calcium signal was modeled as a positively rectifying quadratic operation. Note that the central "high-pass filters" had a small low-passed component to allow sustained responses in the models (40) (*SI Appendix*). (*B*) The unmodified (*Top*) and modified (*Bottom*) model responses to stationary sawtooth gradients and a square-wave grating, as in Fig. 2 *E* and *F*. The preferred directions of the models are indicated with arrows. a. u., arbitrary units. (*C*) The unmodified (*Top*) and modified (*Bottom*) model responses to gray–black and white–gray square-wave gratings, as in Fig. 3*A*. The preferred direction of each model was rightward. (*D*) The unmodified (*Top*) and modified (*Bottom*) model responses to pairs of bars, either over time (*Left*) or averaged over time (*Right*), as in Fig. 3 *B* and *C*. The preferred direction of each model was rightward.

Manipulating the Illusory Motion Percept by Selective Silencing of T4 or T5 Neurons. How might the pattern of edge responses in T4 and T5 neurons (Fig. 2 and *SI Appendix*, Fig. S2) explain illusory motion perception in flies (Fig. 1*D*)? Optomotor turning behavior reflects the net responses of neurons tuned to right- and leftward motion, integrated over space (14, 25) (Fig. 5*A* and *SI Appendix*, Fig. S6). Each stationary contrast edge activates a pair of T4 and T5 neurons tuned to opposite directions (Figs. 2 *C* and *E* and 3*A* and *SI Appendix*, Figs. S2*A* and S3*A*). Therefore, when a fly is presented with a stationary sawtooth gradient, T4 neurons drive turning in one direction (toward the lighter shade along the shallow gradient), and T5 neurons drive turning in the opposite direction (toward the darker shade) (Fig. 5*A* and *SI Appendix*, Fig. S6). As a consequence, if there is a systematic imbalance in the contributions of T4 and T5 neurons to the optomotor response, the stationary sawtooth gradient would trigger turning. Our observation that flies turned toward the lighter shade indicates that the contribution of T4 neurons slightly outweighs that of T5 neurons, consistent with previous reports (14, 42, 43). It is important to note that most visual scenes contain similar numbers of edges with positive and negative spatial derivatives, and would therefore activate similar numbers of T4 and T5 neurons tuned to each direction. This within-cell–type symmetry would prevent flies from turning in response to most stationary scenes, even when T4 and T5 neurons influence behavior with different weights.

Based on this explanation, we reasoned that we could manipulate responses to the sawtooth stimulus by using genetic silencing to alter the imbalance between the outputs of T4 and T5 neurons. We hypothesized that silencing T5 neurons would lead to stronger turning toward the light shade (reflecting the remaining T4 neuron signals) (Fig. 5*B* and *SI Appendix*, Fig. S6), while silencing T4 neurons would lead to stronger turning toward the dark shade (reflecting the remaining T5 neuron signals) (Fig. 5*C* and *SI Appendix*, Fig. S6). To test these predictions, we measured turning responses to stationary sawtooth gradients while selectively silencing either T4 or T5 neurons with *shibire*^{ts}. As predicted by this simple model, T5-silenced flies showed enhanced turning toward the light shade of the gradient (Fig. 5*D*), while T4-silenced flies showed an inverted-motion percept and turned toward the dark shade of the gradient (Fig. 5*E*). In addition, silencing T4 neurons affected the turning amplitude more than silencing T5 neurons (*SI Appendix*), consistent with T4 neurons contributing more to the optomotor response than T5 neurons. Thus, these silencing results support this proposed model.

Manipulating Illusory Motion Percepts in Humans by Polarity-Specific Adaptation to Moving Edges. There are three key ingredients for this model of illusory motion perception in flies: 1) distinct light and dark edge motion detectors that contribute differentially to behavior; 2) their selective responses to stationary edges; and 3) subtraction of motion signals with opposite directional tuning. Interestingly, these ingredients are all reported to exist in humans as well: First, there are motion-detecting neurons in

Downloaded at Palestinian Territory, occupied on December 6, 2021
www.manaraa.com

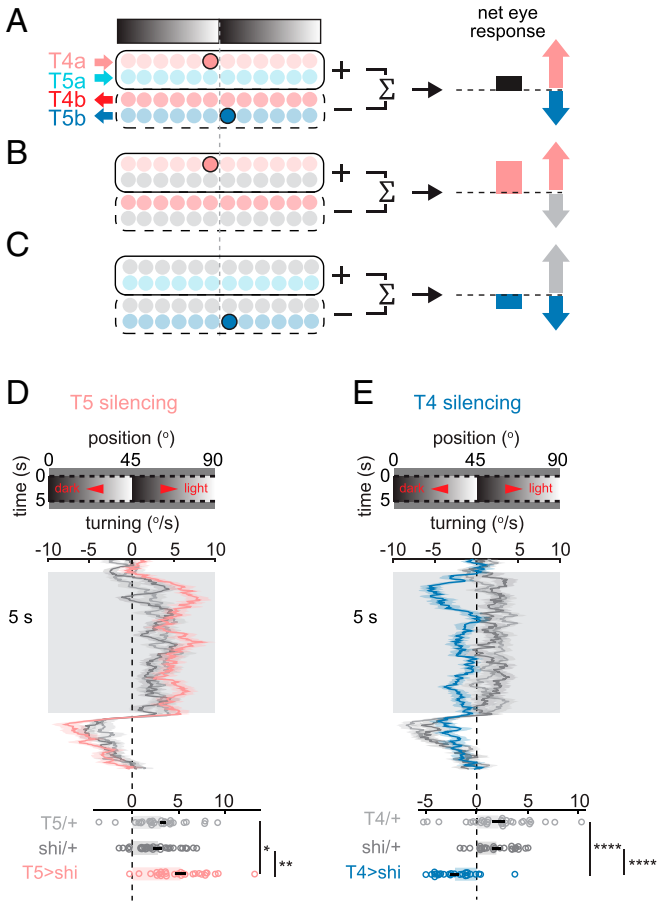

Fig. 5. Manipulating the illusory motion percept by selective silencing of T4 or T5 neurons. (*A*) Model relating optomotor turning to the responses of T4 and T5 neurons to stationary sawtooth gradients. Only the right eye is depicted here (see also *SI Appendix*, Fig. S6). The net turning response corresponds to the difference of activities between rightward-tuned (T4a, T5a) and leftward-tuned (T4b, T5b) neurons. The sawtooth grating shown elicits activity in T4a and T5b neurons, which drive flies to turn in opposite directions. The direction of turning in wild-type flies (Fig. 1*D*) suggests a greater contribution of T4 than T5 neurons to turning. (*B* and *C*) This model predicts that selective silencing of T5 neurons will enhance turning (*B*), while silencing T4 neurons will reverse turning direction (*C*). (*D* and *E*) Average turning time traces (*Top*; mean ± SEM) and time-averaged responses (*Bottom*) during stationary sawtooth gradient presentation, in (*D*) T5-silenced or (*E*) T4-silenced flies, and in control flies. Bars with error bars indicate mean ± SEM; $n = 28$, 26, and 28 flies for T5-silenced, Gal4 control, and UAS control, respectively; $n = 25$, 31, and 24 flies for T4-silenced, Gal4 control, and UAS control, respectively. $^{*}P \leq 0.05$, $^{**}P \leq 0.01$, $^{****}P \leq 0.0001$ by a Wilcoxon rank-sum test across flies.

primate V1 that respond selectively to light and dark edges (44, 45). In humans, these can be independently adapted to alter motion perception (43, 46). Second, models of motion detection often used in humans and primates, including motion energy models and inhibitory veto mechanisms (47, 48), can respond selectively to specific edge types, similar to T4 and T5 neurons (*SI Appendix*, Fig. S5). Third, subtraction between signals with opposite directional tuning occurs in the middle temporal visual area (MT) (49, 50).

Because humans possess the ingredients of the illusory mechanism in flies, it is possible that a similar mechanism could underlie illusory motion percepts in humans as well. One cannot silence cells in humans, but instead it is possible to use different visual adaptors to selectively reduce the response gains of light vs. dark edge motion detectors (43, 46). Since human visual systems have many neurons with a diversity of tuning properties (51), it seems unlikely that the adaptation paradigm would generate the identical phenotypes as the cell-specific, strong silencing of one of only two classes of primary directional neurons in the fly. Nonetheless, if human illusory perception uses a similar mechanism to flies, then selective adaptation to light or dark edges should differentially affect the magnitude and direction of the illusory motion percepts, similar to silencing of T4 or T5 in flies. Importantly, existing accounts of the illusion do not predict that adaptation of light or dark moving edge detectors would yield differential changes in the illusory velocity, since they do not invoke light and dark pathway splitting.

Thus, to test our fly-inspired mechanistic model in humans, we presented human observers with an adaptor stimulus, followed by a circular sawtooth gradient, which rotated with various slow velocities about a fixation point at its center (Fig. 6 *A* and *B*) (52). The observer made a two-alternative forced choice on the perceived direction of the rotation (clockwise or counterclockwise), and a sigmoidal psychometric curve was fitted to their responses. The perceived velocity of the illusory motion was computed as the opposite of the motion-nulling rotational velocity, at which the observer reported motion in each direction with equal probability. Before the test stimulus was presented, circular adaptor stimuli were presented, containing either uniform gray, rotating light edges, or dark edges (Fig. 6 *A* and *B* and Movie S3). The edge adaptor stimuli moved in alternating directions to avoid directional motion aftereffects.

Adaptation to each edge type shifted the velocity of illusory motion negatively (Fig. 6 *C* and *D*) but adaptation to light edges did so significantly more, paralleling the stronger effect of T4 relative to T5 silencing in flies (Fig. 5). In more than half of the participants, the direction of the illusion was inverted after being adapted to moving light edges (Fig. 6 *C* and *D* and *SI Appendix*, Fig. S7), again similar to T4-silenced flies (Fig. 5*E*). These asymmetric effects of light and dark edges are unlikely to be due to differential effectiveness of the two adaptor edge types, since the slope of the psychometric curve (namely, the sensitivity) was similarly reduced by both edge types (Fig. 6*E*). Overall, the adaptation effects in humans are consistent with a mechanism in which the illusory motion percept arises from imbalances in subtractive interactions among polarity-selective edge responses of direction-selective neurons.

Discussion

Our results demonstrate that *Drosophila*, like humans and other vertebrates, can perceive motion in stationary patterns (Fig. 1). The motion detectors T4 and T5 are necessary for the illusory percept (Figs. 1 and 5), and those neurons respond to the sharp stationary edges of the sawtooth pattern that triggers the illusion (Fig. 2 and *SI Appendix*, Fig. S2). The stationary edge responses in T4 and T5 neurons emerge through distinct phenomenology, despite the similarity in the two neuron types' responses to sharp edges (Fig. 3 and *SI Appendix*, Fig. S3). A minimal synaptic model captured the stationary edge responses of T4 (Fig. 4). Polarity-selective stationary edge responses of T4 and T5 neurons, their imbalanced contributions to behavior, and subtraction of motion signals with opposite directional tuning were sufficient to explain the illusion in flies. This proposed mechanism allowed us to predictably manipulate the illusory motion percept of flies by selective silencing of T4 or T5 neurons (Fig. 5). These experiments showed that the illusory motion caused by stationary luminance gradients arose from an imperfect cancellation of direction-selective neuron responses to sharp contrast edges. Last, we presented human psychophysical results that suggest that the illusory percept in humans could result from a mechanism similar to that in flies (Fig. 6).

Downloaded at Palestinian Territory, occupied on December 6, 2021

www.manaraa.com

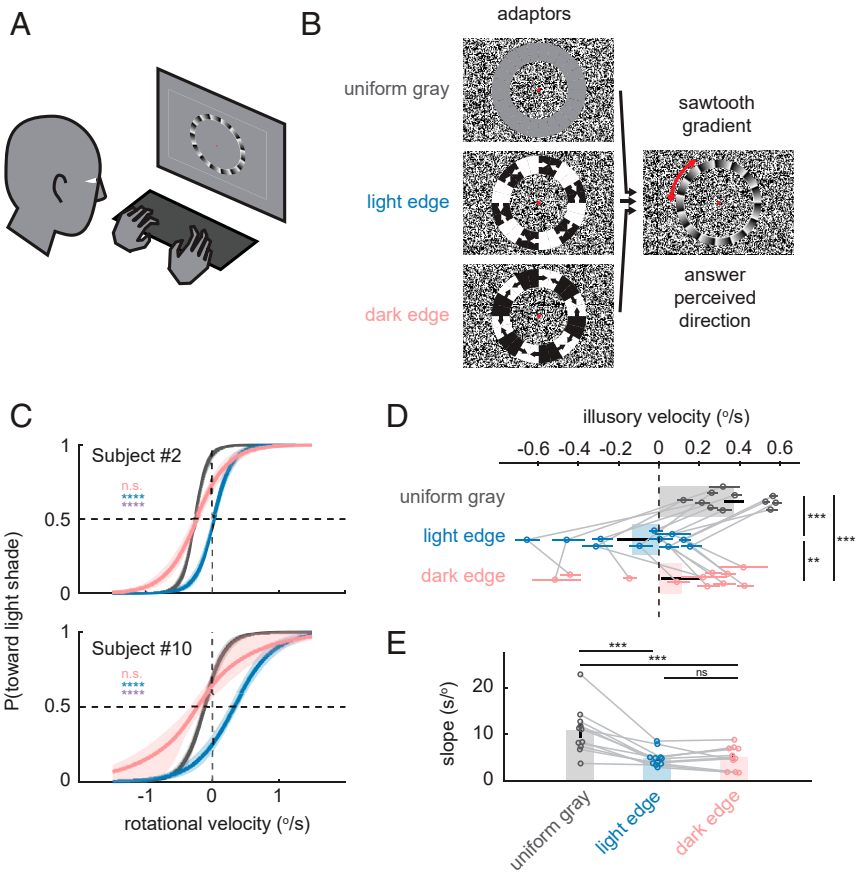

Fig. 6. Manipulating illusory motion in humans by polarity-specific adaptation to moving edges. (*A*) Subjects viewed visual stimuli on a liquid crystal display monitor and reported the perceived direction of rotation by button presses. (*B*) Schematics of the visual stimuli used. See also Movie S3. Adaptor stimuli contained uniform gray or rotating light or dark edges, which alternated direction of motion. Adaptors were followed by a 0.5-s presentation of a slowly rotating sawtooth gradient, whose perceived direction subjects reported (*SI Appendix*). (*C*) Psychometric curves for two representative subjects by adaptor conditions. Each curve shows the estimated probability that the subject sees rotation toward the light shade along the shallow gradient, as a function of added rotational velocity (positive velocity indicates rotation toward the light shade). The velocity that gives 0.5 probability on each psychometric curve is the nulling velocity, which corresponds to the negative of the estimated velocity of illusion. The curves were drawn using the means of the joint posterior distributions of the threshold and slope of logistic psychometric functions, with 68% credible intervals. (*D*) Estimated mean illusory motion velocity by adaptor conditions, color-coded as in *C*. Error bars around individual data points correspond to 68% credible intervals, and error bars on the bar plots are SEs of group mean. Data from the same subject are connected by gray lines. (*E*) Estimated mean slope by adaptor conditions; $n = 11$. (*C*) n.s., nonsignificant; $^{****}P \leq 0.0001$, analytically calculated probability that a pair of posterior distributions of illusory velocity are not different (*SI Appendix*). Blue stars indicate tests between uniform gray and light edge conditions, pink between uniform gray and dark edges, and violet between light and dark edges. (*D* and *E*) $^{**}P \leq 0.01$, $^{***}P \leq 0.001$ by a Wilcoxon signed-rank test.

Synaptic Mechanisms of Stationary Edge Responses in T4 and T5. We found that different phenomenologies are associated with the stationary edge responses in T4 and T5 (Fig. 3 and *SI Appendix*, Fig. S3), in contrast to the previously noted striking parallels between the two neuron types (14, 15, 25–29, 31, 32, 35, 39). In particular, while nonpreferred dark contrast on the preferred side was necessary to drive stationary edge responses in T4 neurons (Fig. 3 *A*–*C* and *SI Appendix*, Fig. S3 *A*–*E*), preferred dark contrast was sufficient to explain T5's stationary edge responses (Fig. 3 *A*, *D*, and *E* and *SI Appendix*, Fig. S3 *A* and *F*–*I*). This result in T4 is surprising, since T4 receives major excitatory inputs only from ON cells (35, 37, 53). In addition to these, on the preferred side of its dendritic arbor, T4 receives synapses from Mi4 and CT1 cells, which are inhibitory ON cells (27, 34–37, 41). In our computational model of T4, introducing low baseline activity to the arm corresponding to Mi4/CT1 was enough to replicate the counterintuitive response of T4 to the half-contrast square-wave gratings (Figs. 3*A* and 4*H* and *SI Appendix*, Fig. S3*A*). The baseline activity in the Mi4/CT1 arm allows dark contrast on the preferred side to disinhibit T4, while it reduces T4 responses to stimuli that only consist of contrast increments (e.g., the white–gray grating). The assumption that Mi4 can be inhibited by contrast decrement is also consistent with previous Mi4 measurements (27). Interestingly, enhancement of T4 activity by a dark bar on the preferred side in the presence of a light bar at the RF center (Fig. 3 *B* and *C* and *SI Appendix*, Fig. S3 *B*–*E*) was also observed in the T4 model without baseline excitation in the Mi4/CT1 arm (Fig. 4*C*). This was because the light bar at the center, after spatial low-pass filtering, can slightly excite the Mi4/CT1 arm, effectively serving as baseline excitation.

Unlike T4, the response of T5 was generally not affected by its nonpreferred contrast (light contrast), consistent with the lack of ON inputs into T5 (34, 35) (Fig. 3 and *SI Appendix*, Fig. S3). Instead, dark bars on either side of the RF center suppressed the response of T5, with preferred side inhibition being stronger. While it is presumed that T5 receives OFF inhibitory signals from CT1 at the preferred side of its RF (35, 41), no inhibitory input to the null side of the T5 RF has been identified. One possible source of the unexpected null-side inhibition in T5 is suppression of its excitatory inputs (Tm1, 2, 4, and 9) by a center-surround

Downloaded at Palestinian Territory, occupied on December 6, 2021
www.manaraa.com

antagonistic interaction (*SI Appendix*, Fig. S4*H*). Consistent with this idea, Tm1, 2, 4, and 9 are all reported to have an inhibitory lobe of spatial RF spanning about 10° (34).

Sensitivity to Gradients Is Incorporated into Direction-Selective Signals. Studies using reverse-phi apparent motion stimuli have shown that T4 responds most strongly to a dark bar followed by a bright bar displaced toward the null direction, and T5 to a bright bar followed by a dark bar (27, 42, 54). The spatial contrast organization of the reverse-phi pairing preferred by T4 cells is consistent with the configurations of stationary contrast edges (Fig. 2 and *SI Appendix*, Fig. S2) and bar pairs (Fig. 3 and *SI Appendix*, Fig. S3) that generated the largest responses in T4 in the present study. This suggests that selective responses to specific spatial gradients may enhance responses to specific spatiotemporal correlations.

Gradient detectors are the optimal velocity estimators when the signal to noise of inputs is high (55). These detectors compute input velocity by dividing local temporal luminance derivatives by local spatial luminance derivatives. When signal to noise is low, the optimal detector becomes a product rather than a ratio of these two terms, which is equivalent to a Hassenstein–Reichardt correlator-like model (55). The sensitivity to gradients measured in T4 and T5 therefore looks like the spatial derivative terms that exist in this formulation of an optimal model. It will be interesting to assess how closely the algorithms implemented in T4 and T5 direction selectivity relate to optimal models of motion detection (56–58).

Effects of Selective Adaptation and Diverse Neural Tuning in Humans. In humans, selective adaptation to moving light or dark edges changed illusory motion percepts in ways similar to silencing T4 or T5 neurons in flies, especially in terms of their differential magnitudes (Figs. 5 and 6). However, the parallel was not perfect. Most notably, adaptation to dark moving edges reduced, rather than increased, the illusory velocity in most subjects, unlike silencing of T5 neurons in flies (Figs. 5*D* and 6 *D* and *E* and *SI Appendix*, Fig. S7). The observed reduction in the illusory velocity by either type of adaptor cannot be simply attributed to a general reduction of gain in direction-selective neurons. This is because the illusory velocity is measured as the physical nulling velocity. In this protocol, if an omnidirectional moving adaptor uniformly decreased the gain of all direction-selective neurons regardless of their tuning, then stationary sawtooth gradients would evoke overall smaller neural activity in the direction-selective cells, and result in a reduced illusory motion percept. However, with the globally reduced gain, there would be no expected decrease in the amount of physical motion required to cancel the motion percept (i.e., the nulling velocity). Therefore, any change in the magnitude of illusory motion by adaptation must be a result of altered balance among differently tuned direction-selective neurons.

What differences between direction-selective neurons in flies and humans could explain the observed discrepancy between the effects of cell silencing and of adaptation? One potential source of the discrepancy is the more diverse spatial frequency tuning of primate direction-selective cells compared with *Drosophila* T4 and T5. Unlike T4 and T5 neurons, whose receptive fields have a fixed spatial scale (~15°) determined by their stereotypical morphology (35), V1 simple cells in the primate brain have spatial frequency tuning that spans four octaves (51, 59). As a result, subpopulations of simple cells would likely prefer the sloped portion of the sawtooth gradient over sharp edges, violating our assumption that only a pair of detector types with opposite light/dark and directional preferences is responding strongly to the sawtooth gradient (Fig. 5*A*). To fully explain the phenomenology of the human adaptation experiments, it seems necessary to incorporate interactions between the spatial frequency tuning and selectivity to contrast polarity or susceptibility to adaptation. Indeed, such an interaction between spatial frequency tuning and contrast polarity has been reported in mammalian V1 (60).

Relationship to Existing Theories of Peripheral Drift Illusion in Humans. Our account for the illusory motion, based on imbalances between contrast polarity-selective motion-detecting neurons, differs critically from existing theories of the illusion in humans (2, 9, 10), in that it attributes the illusion to the architecture of the motion detection circuitry itself. However, our account is not contradictory, but rather complementary, to the existing theories. For example, previous studies in humans have attributed the illusory motion in the peripheral drift illusion to retinal motion caused by microsaccades (10, 11), while it remained unclear why an illusion resulting from eye movements that are on average isotropic is directionally biased. The imbalanced contribution between light and dark edge-selective motion detectors proposed here could be the source of this break in symmetry.

Competition between contrast polarity-selective motion-detecting neurons could also potentially account for several other aspects of the phenomenology of peripheral drift illusions in humans. For example, several studies have observed dimorphism among individuals in the direction of the illusory motion perceived in the sawtooth gradient stimuli (3, 61) (although we did not replicate this observation; Fig. 6 and *SI Appendix*, Fig. S6). Variation in weighting between light and dark edge motion-detecting neurons among individuals or due to viewing conditions could explain this dimorphism. In addition, the direction of illusory motion caused by the sawtooth gradients depends on their luminance relative to the background in humans (62). The opposite illusory motion percepts caused by light and dark gradients parallel how, in flies, T4 and T5 drive turning in opposite directions in response to sawtooth gradients. Thus, this phenomenology is broadly consistent with the idea that contrast polarity-selective motion-detecting neurons are driving peripheral drift illusions in humans.

Illusions and Efficient Motion Detection in Natural Environments. The parallels in effects on the illusory motion percept of selective silencing of T4 or T5 in flies (Fig. 5) and selective adaptation to moving light and dark edges in humans (Fig. 6) suggest that similar mechanisms may underlie the illusion in both organisms. Considering the vast evolutionary distance between humans and flies, the shared ingredients of the illusory motion between flies and vertebrates—separate light and dark edge motion detectors (44, 45, 63, 64) and the asymmetry among them (43, 46, 65), subtraction among oppositely direction-tuned neurons (49, 50)—likely reflect convergent strategies for efficient motion detection in natural environments. First, pathway splitting by contrast polarity can improve the efficiency of contrast encoding (66), and can easily result in polarity-selective motion signals. Second, the asymmetric weighting of light and dark edge motion channels is closely tied to performance of motion detection algorithms in natural scenes (43, 56, 57, 67, 68). Natural scenes contain asymmetries in light and dark contrasts (69), and motion detection algorithms can generically incorporate asymmetric processing to improve motion estimates (57). The similarities between fly and human motion percepts in response to stationary patterns suggest that invertebrate and vertebrate visual systems incorporate light–dark asymmetries into motion signals in similar ways (43, 70). Third, the subtractive interaction between direction-selective neurons with opposite directional tuning has been shown to increase selectivity to specific optic flow patterns (71). Our results suggest that the subtractive interaction also plays a critical role in rejecting responses to stationary contrasts that exist in early direction-selective signals (72).

Downloaded at Palestinian Territory, occupied on December 6, 2021

www.manaraa.com

Since the era of Gestalt psychologists, visual illusions have motivated systematic investigations into visual perception (1). However, it has been technically challenging to obtain a satisfactory mechanistic understanding of illusions in humans or other vertebrates. Here, using *Drosophila* as a model system, we characterized the mechanism of a long-known illusory motion percept in enough detail that we could genetically manipulate the direction of the perceived motion. This mechanistic understanding of the illusion in flies provided insights into the illusion in humans, as well. Our results show that these illusory motion percepts reflect deep evolutionary parallels in the architecture for motion detection across phyla.

Materials and Methods

Briefly, in flies, visual stimuli for both the behavioral and imaging experiments were projected onto panoramic screens surrounding the flies using digital light projectors (8, 25). In behavioral experiments, female *Drosophila* flies were tethered to surgical needles and placed on top of air-supported balls, and their walking responses to visual stimuli were measured by rotation of the balls (8, 25). In imaging experiments, visual responses of T4 and T5 neurons expressing the calcium indicator GCaMP6f (24) were measured using two-photon microscopy. In imaging experiments, 5°-wide white or black vertical bars were presented at various azimuthal locations, and the RF center location of each T4 and T5 was estimated post hoc as the location that elicited the strongest responses (27). The responses of T4 and T5 neurons to other stimuli were then aligned with the estimated RF center. Computational models were numerically simulated on Matlab with resolutions of 0.1° and 240 Hz (33, 39). All participants in human psychophysics experiments provided written informed consent and were compensated for participation in the experiment. The experimental protocol was approved by the Institutional Review Board of Yale University and was in accordance with the Declaration of Helsinki. The magnitude of illusory motion was measured as the physical rotational velocity of the pattern that canceled the perceived motion using a Bayesian adaptive method (73). Throughout, the *P* values presented are results of either Wilcoxon rank-sum (fly experiments, except Fig. 1*D*) or signed-rank (Fig. 1*D* and human experiments) tests.

Data Availability. Detailed materials and methods are reported in *SI Appendix*. All experimental data are available in Dryad (https://doi.org/10.5061/dryad.vt4b8gtpd), and scripts to analyze the data and run the computational models are available in GitHub (https://github.com/ClarkLabCode/IllusionPaperCode).

ACKNOWLEDGMENTS. We thank Nicholas Turk-Browne for helpful advice on human psychophysics experiments and for access to the experimental setup in his laboratory. We are indebted to Jonathan B. Demb, James E. Fitzgerald, Anirvan Nandy, and members of the D.A.C. laboratory for helpful comments and discussions. M.A. was supported by the E. Mathilda Ziegler Foundation for the Blind. R.T. was supported by the Takenaka Foundation and the Gruber Foundation. E.S.-G. was supported by a National Defense Science and Engineering Graduate Research Fellowship. D.A.C. and this project were supported by NIH Grants R01EY026555, NIH P30EY026878, and NSF IOS1558103, a Searle Scholar Award, a Sloane Foundation Fellowship, the Smith Family Foundation, and the E. Mathilda Ziegler Foundation for the Blind.

1. D. M. Eagleman, Visual illusions and neurobiology. *Nat. Rev. Neurosci.* **2**, 920–926 (2001).
2. J. Faubert, A. M. Herbert, The peripheral drift illusion: A motion illusion in the visual periphery. *Perception* **28**, 617–621 (1999).
3. A. Fraser, K. J. Wilcox, Perception of illusory movement. *Nature* **281**, 565–566 (1979).
4. A. Kitaoka, H. Ashida, Phenomenal characteristics of the peripheral drift illusion. *Vision* **15**, 261–262 (2003).
5. C. Agrillo, S. Gori, M. J. Beran, Do rhesus monkeys (*Macaca mulatta*) perceive illusory motion? *Anim. Cogn.* **18**, 895–910 (2015).
6. R. Bååth, T. Seno, A. Kitaoka, Cats and illusory motion. *Psychology* **05**, 1131–1134 (2014).
7. S. Gori, C. Agrillo, M. Dadda, A. Bisazza, Do fish perceive illusory motion? *Sci. Rep.* **4**, 6443 (2014).
8. M. S. Creamer, O. Mano, R. Tanaka, D. A. Clark, A flexible geometry for panoramic visual and optogenetic stimulation during behavior and physiology. *J. Neurosci. Methods* **323**, 48–55 (2019).
9. B. R. Conway, A. Kitaoka, A. Yazdanbakhsh, C. C. Pack, M. S. Livingstone, Neural basis for a powerful static motion illusion. *J. Neurosci.* **25**, 5651–5656 (2005).
10. I. Murakami, A. Kitaoka, H. Ashida, A positive correlation between fixation instability and the strength of illusory motion in a static display. *Vision Res.* **46**, 2421–2431 (2006).
11. J. Otero-Millan, S. L. Macknik, S. Martinez-Conde, Microsaccades and blinks trigger illusory rotation in the "rotating snakes" illusion. *J. Neurosci.* **32**, 6043–6051 (2012).
12. H. H. Yang, T. R. Clandinin, Elementary motion detection in *Drosophila*: Algorithms and mechanisms. *Annu. Rev. Vis. Sci.* **4**, 143–163 (2018).
13. D. A. Clark, J. B. Demb, Parallel computations in insect and mammalian visual motion processing. *Curr. Biol.* **26**, R1062–R1072 (2016).
14. M. S. Maisak *et al*., A directional tuning map of *Drosophila* elementary motion detectors. *Nature* **500**, 212–216 (2013).
15. M. S. Creamer, O. Mano, D. A. Clark, Visual control of walking speed in *Drosophila*. *Neuron* **100**, 1460–1473.e6 (2018).
16. T. Schilling, A. Borst, Local motion detectors are required for the computation of expansion flow-fields. *Biol. Open* **4**, 1105–1108 (2015).
17. E. Buchner, Elementary movement detectors in an insect visual system. *Biol. Cybern.* **24**, 85–101 (1976).
18. K. G. Götz, H. Wenking, Visual control of locomotion in the walking fruitfly *Drosophila*. *J. Comp. Physiol.* **85**, 235–266 (1973).
19. P. J. Hsieh, G. P. Caplovitz, P. U. Tse, Illusory motion induced by the offset of stationary luminance-defined gradients. *Vision Res.* **46**, 970–978 (2006).
20. H. Bülthoff, K. G. Götz, Analogous motion illusion in man and fly. *Nature* **278**, 636–638 (1979).
21. A. Bahl, G. Ammer, T. Schilling, A. Borst, Object tracking in motion-blind flies. *Nat. Neurosci.* **16**, 730–738 (2013).
22. J. S. Kain, C. Stokes, B. L. de Bivort, Phototactic personality in fruit flies and its suppression by serotonin and white. *Proc. Natl. Acad. Sci. U.S.A.* **109**, 19834–19839 (2012).
23. T. Kitamoto, Conditional modification of behavior in *Drosophila* by targeted expression of a temperature-sensitive shibire allele in defined neurons. *J. Neurobiol.* **47**, 81–92 (2001).
24. T.-W. Chen *et al*., Ultrasensitive fluorescent proteins for imaging neuronal activity. *Nature* **499**, 295–300 (2013).
25. E. Salazar-Gatzimas *et al*., Direct measurement of correlation responses in *Drosophila* elementary motion detectors reveals fast timescale tuning. *Neuron* **92**, 227–239 (2016).
26. E. Gruntman, S. Romani, M. B. Reiser, Simple integration of fast excitation and offset, delayed inhibition computes directional selectivity in *Drosophila*. *Nat. Neurosci.* **21**, 250–257 (2018).
27. E. Salazar-Gatzimas, M. Agrochao, J. E. Fitzgerald, D. A. Clark, The neuronal basis of an illusory motion percept is explained by decorrelation of parallel motion pathways. *Curr. Biol.* **28**, 3748–3762.e8 (2018).
28. Y. E. Fisher, M. Silies, T. R. Clandinin, Orientation selectivity sharpens motion detection in *Drosophila*. *Neuron* **88**, 390–402 (2015).
29. E. Gruntman, S. Romani, M. B. Reiser, The computation of directional selectivity in the *Drosophila* OFF motion pathway. *eLife* **8**, 721902 (2019).
30. J. Haag, A. Arenz, E. Serbe, F. Gabbiani, A. Borst, Complementary mechanisms create direction selectivity in the fly. *eLife* **5**, e17421 (2016).
31. J. C. S. Leong, J. J. Esch, B. Poole, S. Ganguli, T. R. Clandinin, Direction selectivity in *Drosophila* emerges from preferred-direction enhancement and null-direction suppression. *J. Neurosci.* **36**, 8078–8092 (2016).
32. J. Haag, A. Mishra, A. Borst, A common directional tuning mechanism of *Drosophila* motion-sensing neurons in the ON and in the OFF pathway. *eLife* **6**, e29044 (2017).
33. J. A. Zavatone-Veth, B. A. Badwan, D. A. Clark, A minimal synaptic model for direction selective neurons in *Drosophila*. *J. Vis.* **20**, 2 (2020).
34. A. Arenz, M. S. Drews, F. G. Richter, G. Ammer, A. Borst, The temporal tuning of the *Drosophila* motion detectors is determined by the dynamics of their input elements. *Curr. Biol.* **27**, 929–944 (2017).
35. K. Shinomiya *et al*., Comparisons between the ON- and OFF-edge motion pathways in the *Drosophila* brain. *eLife* **8**, e40025 (2019).
36. J. A. Strother *et al*., The emergence of directional selectivity in the visual motion pathway of *Drosophila*. *Neuron* **94**, 168–182.e10 (2017).
37. S. Y. Takemura *et al*., The comprehensive connectome of a neural substrate for "ON" motion detection in *Drosophila*. *eLife* **6**, e24394 (2017).
38. V. Torre, T. A. Poggio, A synaptic mechanism possibly underlying directional selectivity to motion. *Proc. R. Soc. Lond. B Biol. Sci.* **202**, 409–416 (1978).
39. B. A. Badwan, M. S. Creamer, J. A. Zavatone-Veth, D. A. Clark, Dynamic nonlinearities enable direction opponency in *Drosophila* elementary motion detectors. *Nat. Neurosci.* **22**, 1318–1326 (2019).
40. R. Behnia, D. A. Clark, A. G. Carter, T. R. Clandinin, C. Desplan, Processing properties of ON and OFF pathways for *Drosophila* motion detection. *Nature* **512**, 427–430 (2014).
41. M. Meier, A. Borst, Extreme compartmentalization in a *Drosophila* amacrine cell. *Curr. Biol.* **29**, 1545–1550.e2 (2019).
42. D. A. Clark, L. Bursztyn, M. A. Horowitz, M. J. Schnitzer, T. R. Clandinin, Defining the computational structure of the motion detector in *Drosophila*. *Neuron* **70**, 1165–1177 (2011).
43. D. A. Clark *et al*., Flies and humans share a motion estimation strategy that exploits natural scene statistics. *Nat. Neurosci.* **17**, 296–303 (2014).
44. P. H. Schiller, B. L. Finlay, S. F. Volman, Quantitative studies of single-cell properties in monkey striate cortex. I. Spatiotemporal organization of receptive fields. *J. Neurophysiol.* **39**, 1288–1319 (1976).
45. P. H. Schiller, Central connections of the retinal ON and OFF pathways. *Nature* **297**, 580–583 (1982).

Downloaded at Palestinian Territory, occupied on December 6, 2021
www.manaraa.com

46. G. Mather, B. Moulden, A. O'Halloran, Polarity specific adaptation to motion in the human visual system. *Vision Res.* **31**, 1013–1019 (1991).
47. E. H. Adelson, J. R. Bergen, Spatiotemporal energy models for the perception of motion. *J. Opt. Soc. Am. A* **2**, 284–299 (1985).
48. H. B. Barlow, W. R. Levick, The mechanism of directionally selective units in rabbit's retina. *J. Physiol.* **178**, 477–504 (1965).
49. N. Qian, R. A. Andersen, Transparent motion perception as detection of unbalanced motion signals. II. Physiology. *J. Neurosci.* **14**, 7367–7380 (1994).
50. E. P. Simoncelli, D. J. Heeger, A model of neuronal responses in visual area MT. *Vision Res.* **38**, 743–761 (1998).
51. K. H. Foster, J. P. Gaska, M. Nagler, D. A. Pollen, Spatial and temporal frequency selectivity of neurones in visual cortical areas V1 and V2 of the macaque monkey. *J. Physiol.* **365**, 331–363 (1985).
52. R. Hisakata, I. Murakami, The effects of eccentricity and retinal illuminance on the illusory motion seen in a stationary luminance gradient. *Vision Res.* **48**, 1940–1948 (2008).
53. F. P. Davis *et al*., A genetic, genomic, and computational resource for exploring neural circuit function. *eLife* **9**, e50901 (2020).
54. M. Joesch, F. Weber, H. Eichner, A. Borst, Functional specialization of parallel motion detection circuits in the fly. *J. Neurosci.* **33**, 902–905 (2013).
55. M. Potters, W. Bialek, Statistical mechanics and visual signal processing. *J. Phys. I* **4**, 1755–1775 (1994).
56. J. E. Fitzgerald, D. A. Clark, Nonlinear circuits for naturalistic visual motion estimation. *eLife* **4**, e09123 (2015).
57. J. E. Fitzgerald, A. Y. Katsov, T. R. Clandinin, M. J. Schnitzer, Symmetries in stimulus statistics shape the form of visual motion estimators. *Proc. Natl. Acad. Sci. U.S.A.* **108**, 12909–12914 (2011).
58. S. R. Sinha, W. Bialek, R. R. de Ruyter van Steveninck, Optimal local estimates of visual motion in a natural environment. arXiv:1812.11878 (31 December 2018).
59. M. S. Silverman, D. H. Grosof, R. L. De Valois, S. D. Elfar, Spatial-frequency organization in primate striate cortex. *Proc. Natl. Acad. Sci. U.S.A.* **86**, 711–715 (1989).
60. J. Kremkow *et al*., Neuronal nonlinearity explains greater visual spatial resolution for darks than lights. *Proc. Natl. Acad. Sci. U.S.A.* **111**, 3170–3175 (2014).
61. G. Naor-Raz, R. Sekuler, Perceptual dimorphism in visual motion from stationary patterns. *Perception* **29**, 325–335 (2000).
62. A. Kitaoka, "The Fraser-Wilcox illusion and its extension" in *The Oxford Compendium of Visual Illusions*, A. G. Shapiro, D. Todorović, Eds. (Oxford University Press, 2017), pp. 500–511.
63. T. Euler, P. B. Detwiler, W. Denk, Directionally selective calcium signals in dendrites of starburst amacrine cells. *Nature* **418**, 845–852 (2002).
64. E. V. Famiglietti, Dendritic co-stratification of ON and ON-OFF directionally selective ganglion cells with starburst amacrine cells in rabbit retina. *J. Comp. Neurol.* **324**, 322–335 (1992).
65. Q. Hu, J. D. Victor, A set of high-order spatiotemporal stimuli that elicit motion and reverse-phi percepts. *J. Vis.* **10**, 1–16 (2010).
66. J. Gjorgjieva, H. Sompolinsky, M. Meister, Benefits of pathway splitting in sensory coding. *J. Neurosci.* **34**, 12127–12144 (2014).
67. J. Chen, H. B. Mandel, J. E. Fitzgerald, D. A. Clark, Asymmetric ON-OFF processing of visual motion cancels variability induced by the structure of natural scenes. *eLife* **8**, e47579 (2019).
68. A. Leonhardt *et al*., Asymmetry of *Drosophila* ON and OFF motion detectors enhances real-world velocity estimation. *Nat. Neurosci.* **19**, 706–715 (2016).
69. W. S. Geisler, Visual perception and the statistical properties of natural scenes. *Annu. Rev. Psychol.* **59**, 167–192 (2008).
70. T. Yildizoglu, C. Riegler, J. E. Fitzgerald, R. Portugues, A neural representation of naturalistic motion-guided behavior in the zebrafish brain. *Curr. Biol.* **30**, 2321–2333.e6 (2020).
71. A. S. Mauss *et al*., Neural circuit to integrate opposing motions in the visual field. *Cell* **162**, 351–362 (2015).
72. N. K. Kühn, T. Gollisch, Activity correlations between direction-selective retinal ganglion cells synergistically enhance motion decoding from complex visual scenes. *Neuron* **101**, 963–976.e7 (2019).
73. L. L. Kontsevich, C. W. Tyler, Bayesian adaptive estimation of psychometric slope and threshold. *Vision Res.* **39**, 2729–2737 (1999).

Downloaded at Palestinian Territory, occupied on December 6, 2021

www.manaraa.com